THE JOURNAL OF PHYSICAL CHEMISTRY C

Article

pubs.acs.org/JPCC

Nitrogen Vacancy-Promoted Photocatalytic Activity of Graphitic Carbon Nitride

Ping Niu, Gang Liu,* and Hui-Ming Cheng

Shenyang National Laboratory for Materials Science, Institute of Metal Research, Chinese Academy of Sciences, 72 Wenhua Road, Shenyang 110016, China

ABSTRACT: Vacancy defects can play an important role in modifying the electronic structure and the properties of photoexcited charge carriers and consequently the photocatalytic activity of semiconductor photocatalysts. By controlling the polycondensation temperature of a dicyandiamide precursor in the preparation of graphitic carbon nitride (g-C_3N_4), we introduced nitrogen vacancies in the framework of g-C_3N_4. These vacancies exert remarkable effects on modifying the electronic structure of g-C_3N_4 as shown in UV−visible absorption spectra and valence band spectra. Steady and time-resolved fluorescence emission spectra show that, due to the existence of abundant nitrogen vacancies, the intrinsic radiative recombination of electrons and holes in g-C_3N_4 is greatly restrained, and the population of short-lived and long-lived charge carriers is decreased and increased, respectively. As a consequence, the overall photocatalytic activity of the g-C_3N_4, characterized by the ability to generate •OH radicals, photodecomposition of Rhodamine B, and photocatalytic hydrogen evolution under both UV−visible and visible light, was remarkably improved.

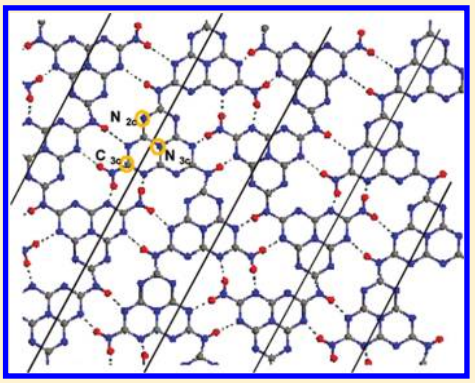

1. INTRODUCTION

Photocatalysis is an attractive yet very challenging process to convert solar energy into chemical energy.[1] One of the central tasks to be solved before its practical application is to develop highly efficient photocatalysts, which can work well under solar light. Various semiconductors including oxides, sulfides, and nitrides have been explored as possible photocatalysts in past decades.[2,3] Metal oxides among them have been most widely investigated due to their valuable physicochemical properties such as proper band edges and good stability for photocatalytic applications. However, the most stable metal oxide photocatalysts (for instance, the prototypical TiO_2) suffer from no or limited visible light absorption due to their large bandgap.[4,5] This is intrinsically caused by the deep valence band consisting of dominant O 2p states. Since N 2p orbits have a higher potential energy than O 2p orbits,[4] a variety of metal nitrides or oxynitrides have a smaller bandgap and thus are increasingly explored as visible light responsive photocatalysts.[6−9] For example, Ta_2O_5 with a bandgap of 4.0 eV only absorbs the light with its wavelength shorter than 310 nm,[10] whereas TaON and Ta_3N_5 with bandgaps of 2.5 and 2.1 eV can absorb visible light with wavelengths up to 500 and 600 nm, respectively.[11] Recently, graphitic carbon nitride (g-C_3N_4), a metal-free photocatalyst, has attracted intensive interest for its promising applications in photosplitting water, photodecomposition of organic pollutants, and photosynthesis under visible light[12,13] because this material has a bandgap of ca. 2.7 eV and consequently can absorb light up to 450 nm.[12]

Although g-C_3N_4 emerges as a good candidate for a visible light photocatalyst, it still suffers from a high recombination probability of photoexcited charge carriers and thus low photocatalytic activity. To improve its photocatalytic activity, many strategies such as controlling shape,[14,15] introducing heteroatoms (B, S, P, and Zn),[16] and coupling with dyes or other semiconductors[17] have been used to modify g-C_3N_4. As a result of these strategies, the activity of g-C_3N_4 has been much improved. To better take advantage of g-C_3N_4, it is important to explore other strategies to further optimize its photoreactivity.

Intrinsic point defects are important for heterogeneous reactions. This is because these defects, which exist in all materials, can modify the electronic structure and also probably act as specific reaction sites for reactant molecules.[18,19] Among the intrinsic point defects of cation vacancies, anion vacancies, and interstitial atoms, the positive role of anion vacancies in affecting the photocatalytic activity of oxide photocatalysts, particularly TiO_2, has been actively pursued.[20−23] It has been demonstrated that oxygen vacancies can not only introduce additional visible light absorption but also increase the UV photocatalytic activity of TiO_2.[20,21] In our previous work,[22] oxygen vacancies were demonstrated to improve the photocatalytic hydrogen evolution of anatase TiO_2 from a mixture of H_2O/methanol. Inspired by these findings in oxides, it is expected that introducing nitrogen vacancies in nitrides may be an effective strategy to optimize the photocatalytic activity of nitrides.

In this work, we used a simple temperature-controlling route to introduce nitrogen vacancies in the framework of polymeric

Received: February 1, 2012
Revised: May 4, 2012
Published: May 4, 2012

dx.doi.org/10.1021/jp301026y | J. Phys. Chem. C 2012, 116, 11013−11018

g-C_3N_4. The effects of nitrogen vacancies on the electronic structure and photocatalytic activities of g-C_3N_4 were investigated. By correlating the modified electronic structure with the improved photocatalytic activity, a strategy to improve the photocatalytic activity of g-C_3N_4 by nitrogen vacancies was established. The results obtained may provide an important indication of how to promote the photocatalytic activity of not only g-C_3N_4 but also other nitride-based photocatalyts.

2. EXPERIMENTAL SECTION

Sample Preparation. g-C_3N_4 was synthesized according to a procedure described in a previous paper.[24] Dicyandiamide (6 g) (Aldrich, 99%) in an open crucible was heated in static air with a ramp rate of 2.3 °C/min to either 550 or 600 °C where it was held for 4 h. Heating at 550 °C produced a light yellow g-C_3N_4 and at 600 °C an orange nitrogen-deficient g-C_3N_4. The agglomerates were milled into a powder in an agate mortar for further characterization and performance measurements. It should be claimed that the widely used "g-C_3N_4" in the literature is actually nonstoichiometric. Here we use "g-C_3N_4" to describe the products condensed from dicyandiamide just to keep consistent with the general usage.

Characterization. X-ray diffraction (XRD) patterns of the samples were recorded with a Rigaku diffractometer using Cu irradiation. Their morphology was observed by scanning electron microscopy (Nova NanoSEM 430). The Brunauer–Emmett–Teller surface area was determined by nitrogen adsorption–desorption isotherm measurements at 77 K (ASAP 2010). Chemical compositions and valence band spectra of the samples were analyzed using X-ray photoelectron spectroscopy (XPS) (Thermo Escalab 250, a monochromatic Al K_α X-ray source). All binding energies were referenced to the C 1s peak (284.6 eV) arising from the adventitious carbon. The optical absorption spectra of the samples were recorded with a UV–visible spectrophotometer (JASCO V-550). Steady and time-resolved fluorescence emission spectra were recorded at room temperature with a fluorescence spectrophotometer (Edinburgh Instruments, FLSP-920). Fourier transform infrared (FTIR) spectra were recorded on a Bruker Tensor 27. Element analysis was performed on Vario MICRO.

Photocatalytic Activity Measurements. •OH radical reactions were performed as follows: 5 mg of the photocatalyst was suspended in an 80 mL aqueous solution containing 0.01 M NaOH and 3 mM terephthalic acid. Before exposure to light, the suspension was stirred in the dark for 30 min. Then 5 mL of the solution was removed every 5 min and centrifuged for fluorescence spectroscopy measurements.

Photodecomposition reactions of Rhodamine B (RhB) were conducted by adding 50 mg of the photocatalyst to a 100 mL 2×10^{-5} M RhB solution. Before exposure to light, the suspension was stirred in the dark for 15 min. Then 5 mL of the solution was taken out at regular intervals under UV–visible light and visible light ($\lambda > 400$ nm) and centrifuged for UV–visible absorption spectroscopy measurements. No oxygen was bubbled in the suspension during the photoreactions. The concentration of Rhodamine B was determined by monitoring the change of the optical density at 554 nm.

Water splitting reactions were carried out in a top-irradiation vessel connected to a closed-glass gas circulation system. The photocatalyst powder (200 mg) was dispersed in 300 mL of aqueous solution containing 10% triethanolamine scavenger by volume. The deposition of 3 wt % Pt cocatalyst was conducted by directly dissolving H_2PtCl_6 in the above 300 mL reaction solution. The reaction temperature was maintained below 20 °C. The amount of H_2 evolved was determined using gas chromatography.

The light source used in the above experiments was a 300 W Xe lamp (Beijing Trusttech Co. Ltd., PLS-SXE-300UV). UV light was removed with a 400 nm long-pass glass filter.

3. RESULTS AND DISCUSSION

Figure 1 shows XRD patterns of the g-C_3N_4 and nitrogen-deficient g-C_3N_4. Both materials show a typical g-C_3N_4 structure without an impurity phase. In detail, g-C_3N_4 has a layered structure, and the in-plane structure in the layers is composed of the periodically cohered strands of polymeric melon units with NH/NH_2 groups through hydrogen bonding as confirmed by Lotsch et al. (Figure 2).[25] As a result, g-C_3N_4 shows two basic X-ray diffraction peaks at around 27.3° and 13.1°. The former is attributed to the long-range interplanar stacking of aromatic systems identified as the (002) peak;[26] the latter with a much weaker intensity is related to an in-plane structural packing motif, namely, the lattice planes parallel to the *c*-axis as depicted by solid lines in Figure 2.[25] Two important features associated with these two peaks are seen when nitrogen vacancies exist in the g-C_3N_4 framework. One is the shift of the former peak from 27.3° to 27.5°, corresponding to a decrease in the interplanar stacking distance from 0.326 to 0.324 nm. This can be interpreted as an improved interlayer stacking order produced by the higher condensation temperature of 600 °C. Thomas et al.[26] reported a shortest distance of 0.319 nm in well-ordered g-C_3N_4 by isothermally tempering the synthesized carbon nitride in a sealed quartz ampule at 600 °C for 10 h. The other feature is the much weakened and broadened peak at 13.1°, indicating much lowered long-range order of the in-plane structural packing in the g-C_3N_4 sheets. It has been suggested that the temperature limit without depleting the amount of nitrogen in g-C_3N_4 is 600 °C in an open atmosphere.[26] In this case, the direct polycondensation of the dicyandiamide precursor at 600 °C in an open container will certainly result in the partial loss of lattice nitrogen so that the distances between strands will have a wider distribution range. This inevitably lowers the long-range order of the strands, resulting in the decreased intensity.

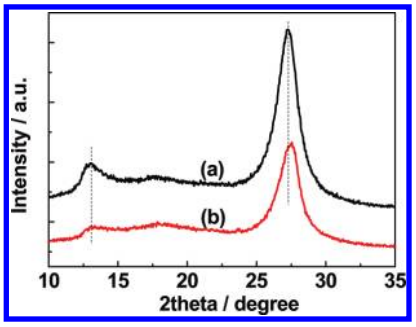

Figure 1. XRD patterns of the (a) g-C_3N_4 and (b) nitrogen-deficient g-C_3N_4 by calcining the dicyandiamide precursor at 550 and 600 °C in static air, respectively.

To further reveal the atomic structure changes of nitrogen-deficient g-C_3N_4, X-ray photoelectron spectroscopy was used to investigate the chemical states of carbon and nitrogen as shown in Figure 3. Typical g-C_3N_4 gives a major N 1s signal peak centered at 398.6 eV and a minor shoulder peak at 400.3 eV, which, respectively, originate from two-coordinated (N_{2c}) and

dx.doi.org/10.1021/jp301026y | J. Phys. Chem. C 2012, 116, 11013–11018

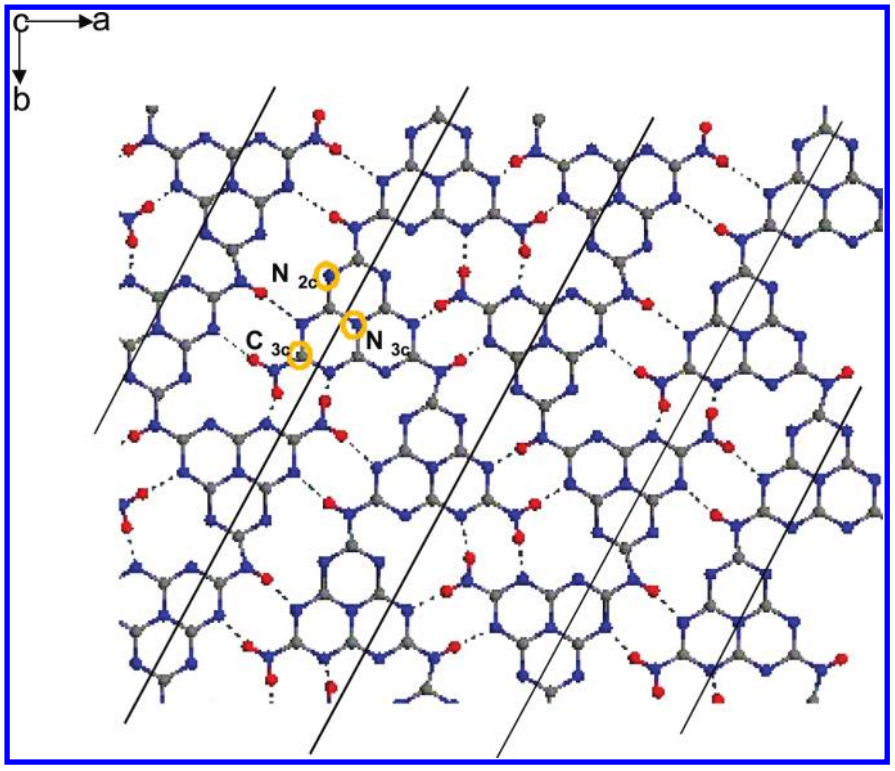

Figure 2. Schematic atomic model of an incompletely condensed graphitic carbon nitride sheet constructed from melon units with NH/NH_2 groups. Two-coordinated nitrogen and three-coordinated nitrogen are labeled as N_{2c} and N_{3c}, and the three-coordinated carbon is labeled as C_{3c}. The solid black lines indicate the periodic structure in-plane.

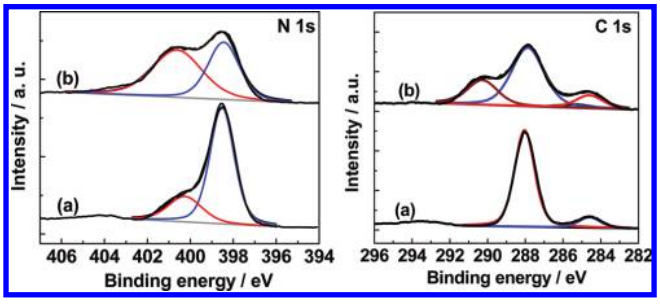

Figure 3. Deconvoluted high-resolution N 1s and C 1s XPS spectra of the (a) g-C_3N_4 and (b) nitrogen-deficient g-C_3N_4.

three-coordinated (N_{3c}) nitrogen atoms in the framework of the heptazine unit (Figure 2). A dominant peak at 288 eV (stemming from the sole three-coordinated carbon (C_{3c})) and an accompanying weak peak at 284.6 eV (arising from the adventitious carbon) appear in the C 1s XPS spectrum. As a result of the formation of nitrogen vacancies, apparent changes occur in both N 1s and C 1s XPS spectra. The N 1s peak from N_{2c} is much weakened so that the peak−area ratio of N_{2c} to N_{3c} decreases from 3.25 to 0.76, clearly indicating that nitrogen vacancies mainly locate at the N_{2c} lattice sites during the condensation. The easier loss of N_{2c} atoms than N_{3c} atoms can be explained in terms of their unsaturated coordination and also higher population. The missing N_{2c} atoms will correspondingly cause the formation of two-coordinated carbon C_{2c} transformed from C_{3c} as confirmed by an additional C 1s peak at 290.3 eV. Furthermore, the N 1s binding energy of N_{3c} shifts from 400.3 to 400.6 eV due to the redistribution of extra electrons left by the missed nitrogen atoms.

The depth distribution of nitrogen vacancies in g-C_3N_4 can be seen by XRD and XPS due to their different detection depths. According to XPS, the surface atomic ratio of carbon to nitrogen increases from 0.72 in the pristine g-C_3N_4 to 0.87 in the nitrogen-deficient g-C_3N_4. The much weakened peak at 13.1° in the XRD pattern clearly suggests that nitrogen vacancies exist not only on the surface but also in the bulk g-C_3N_4, which can be understood as nitrogen atom loss occurring throughout the condensation process of the dicyandiamide precursor. The element analysis demonstrates that ca. 1.9 atom % nitrogen is lost in nitrogen-deficient g-C_3N_4 (a higher preparation temperature, i.e., 620 °C, can lead to a larger amount of nitrogen vacancies, however, which did not bring the further activity increase probably due to the serious destruction of the C−N framework). In addition, the introduced nitrogen vacancies do not obviously change the morphology and particle size of g-C_3N_4, and the specific surface area increases from 12 to 17 m^2/g.

The crystal structure of nitrogen-deficient g-C_3N_4 is basically the same as that of g-C_3N_4 as confirmed by FTIR spectroscopy, though nitrogen vacancies have been introduced in the framework of C−N. The spectra of both g-C_3N_4 and nitrogen-deficient g-C_3N_4 show the typical IR patterns of graphitic carbon nitride. The absorption band at 812 cm^{-1} originates from the bending mode of heptazine rings, indicating the existence of the basic melon units with NH/NH_2 groups.[25] The peaks in the region from 900 to 1800 cm^{-1} can be attributed to either trigonal C−N(−C)−C (full condensation) or bridging C−NH−C units.[25] The broad peaks at around 3000−3500 cm^{-1} reveal the existence of incompletely condensed secondary and primary amines (and their intermolecular hydrogen bonding).[25,27,28] Some peaks below 2000 cm^{-1} shift by ca. 5 cm^{-1} toward low frequency, largely caused by the introduced nitrogen vacancies. In addition, it should be pointed out that we cannot completely rule out the

dx.doi.org/10.1021/jp301026y | J. Phys. Chem. C 2012, 116, 11013−11018

possibility of the formation of higher condensed C_3N_4 as a result of the loss of the NH_3 group during the condensation, which can also be responsible for a lower nitrogen concentration.

The change in the electronic band structure of g-C_3N_4 caused by the introduction of nitrogen vacancies was investigated by UV−visible absorption spectroscopy. As shown in Figure 5A, an additional absorption band ranging from 450 to 600 nm is formed in the nitrogen-deficient g-C_3N_4 compared to the g-C_3N_4. Further analysis using the transformed Kubelka−Munk function versus the energy of the light absorbed shows that the intrinsic bandgap decreases from 2.74 to 2.66 eV as a result of nitrogen vacancies. Similar optical absorption changes were also reported in rutile TiO_2 with bulk oxygen vacancies prepared by the direct thermal oxidation of crystalline TiO or Ti_2O_3 in air.[23] It is well recognized that oxygen vacancies and their related Ti^{3+} in TiO_2 typically generate some localized states at 0.75−1.18 eV below the conduction band.[29] These defect-associated states can even partially overlap the conduction band so that the bandgap can be narrowed when the percentage of oxygen vacancies is high enough.[20] In this case, compared to the smooth signal curve of g-C_3N_4, the nitrogen-deficient g-C_3N_4 shows a rough valence band curve. Some additional electron states appear above the valence band as indicated in the rectangular area in Figure 5. The lost nitrogen atoms leave extra electrons, which are redistributed to their nearest carbon atoms and thus reduce C^{4+} to C^{3+}. The valence band and conduction band of g-C_3N_4 consist of dominant nitrogen p_z and carbon p_z orbitals.[12] In analogy to oxygen-deficient TiO_2, it is reasonable to identify the states observed in the band gap as nitrogen vacancy-related C^{3+} electronic states, which are responsible for the additional absorption band of the nitrogen-deficient g-C_3N_4 in Figure 4.

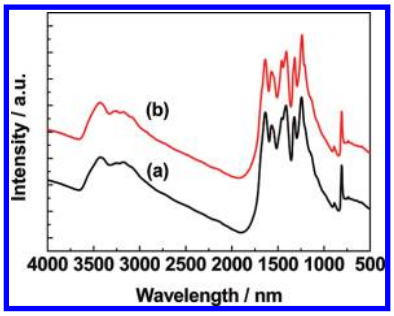

Figure 4. FTIR spectra of (a) g-C_3N_4 and (b) nitrogen-deficient g-C_3N_4.

As demonstrated above, a large amount of nitrogen vacancies existing in the bulk presumably result in a partial overlap of defect-related states with the conduction band. This can explain the slightly narrowed bandgap by nitrogen vacancies in Figure 5.

To investigate the effect of nitrogen vacancies on the photocatalytic activity of g-C_3N_4, we compared the activities of g-C_3N_4 in terms of generating •OH radicals, the photodecomposition of RhB, and photocatalytic hydrogen evolution from a water/triethanolamine solution under both UV−visible and visible light. •OH radicals are considered important oxidative species in decomposing organic molecules.[30] Both photoexcited holes and electrons can cause the formation of •OH radicals by reacting with surface hydroxyl groups and molecular oxygen.[30] The ability of the g-C_3N_4 and nitrogen-

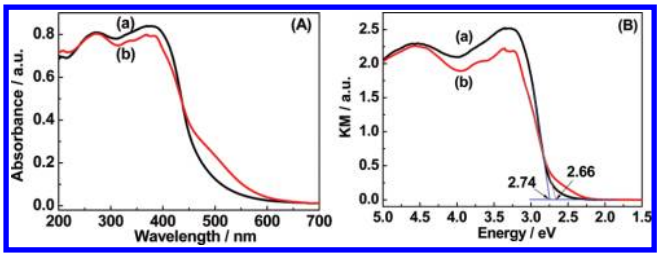

Figure 5. (A) UV−visible absorption spectra and (B) the transformed Kubelka−Munk function vs the energy of the light absorbed of the (a) g-C_3N_4 and (b) nitrogen-deficient g-C_3N_4.

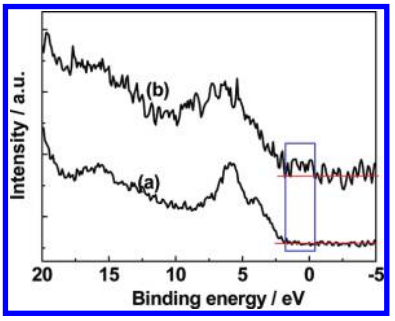

Figure 6. XPS valence band spectra of the (a) g-C_3N_4 and (b) nitrogen-deficient g-C_3N_4.

deficient g-C_3N_4 to generate •OH radicals was estimated by detecting the amount of 2-hydroxy terephthalic acid (TAOH) formed from the reaction of •OH radicals with terephthalic acid (TA).[31] As shown in Figure 7, the fluorescence signal

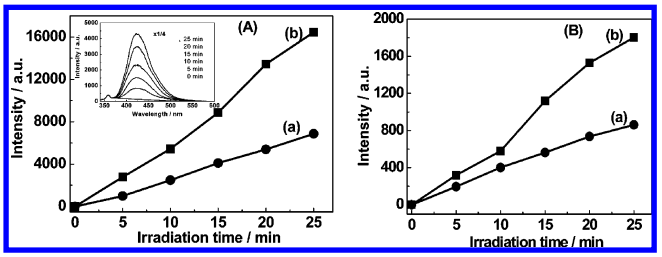

Figure 7. Time-dependent intensity of the fluorescence signal of TAOH at 426 nm generated from the solution of TA by the (a) g-C_3N_4 and (b) nitrogen-deficient g-C_3N_4 under irradiation of (A) UV−visible and (B) visible light (λ > 400 nm). The inset in (A) shows the fluorescence spectra of the TAOH solution generated by the nitrogen-deficient g-C_3N_4.

associated with TAOH continuously increases with irradiation time, suggesting the stability of g-C_3N_4 as a photocatalyst. Furthermore, the nitrogen-deficient g-C_3N_4 shows 2.4 and 2 times higher ability to generate •OH radicals than g-C_3N_4 under both UV−visible and visible light by comparing the time-dependent intensity of the fluorescence signal of TAOH at 426 nm.

The activities of the two materials were further estimated by monitoring the photodecomposition of RhB, as shown in Figure 8. The nitrogen-deficient g-C_3N_4 shows a much superior activity in decomposing RhB under both UV−visible and visible light. For instance, it can completely decompose RhB within 30 min under UV−visible light, while only around 30% RhB can be decomposed by g-C_3N_4 under the same conditions; under visible light it can completely decompose of RhB in 50 min, whereas for g-C_3N_4 it takes as long as 100 min. The

dx.doi.org/10.1021/jp301026y | J. Phys. Chem. C 2012, 116, 11013−11018

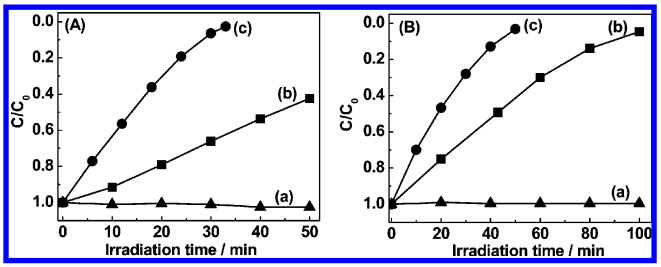

Figure 8. Time dependence of the photodecomposition of RhB under (A) UV−visible and (B) visible light (λ > 400 nm): (a) no photocatalyst; (b) g-C_3N_4; (c) nitrogen-deficient g-C_3N_4.

photocatalytic activity improvement of decomposing RhB is basically consistent with the increased ability to generate •OH radicals by introducing nitrogen vacancies. The superior photocatalytic activity of the nitrogen-deficient g-C_3N_4 to g-C_3N_4 can also be confirmed by detecting hydrogen evolution from a water/triethanolamine mixture. The nitrogen-deficient g-C_3N_4 gives hydrogen evolution rates of 455 and 123 μmol $h^{-1}g^{-1}$ under UV−visible and visible light, but the corresponding rates are 264 and 69 μmol $h^{-1}g^{-1}$ for g-C_3N_4.

Clearly, the photocatalytic activity of g-C_3N_4 can be substantially improved by introducing nitrogen vacancies. To better understand how the nitrogen vacancies affect the photocatalytic activity of g-C_3N_4, we investigated the photophysical processes of g-C_3N_4 and nitrogen-deficient g-C_3N_4. As shown in Figure 9, the nitrogen-deficient g-C_3N_4 gives a similar

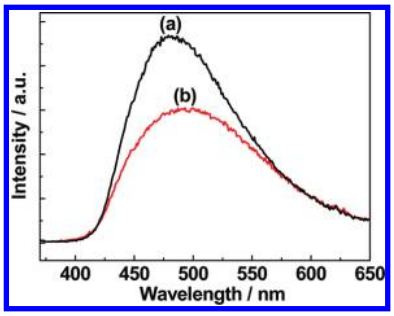

Figure 9. Fluorescence emission spectra of the (a) g-C_3N_4 and (b) nitrogen-deficient g-C_3N_4. The wavelength of excitation light for fluorescence emission spectra was 330 nm.

band-to-band fluorescence emission characteristic to g-C_3N_4. The much weakened emission intensity, however, suggests a greatly decreased radiative recombination probability of photoexcited charge carriers in the nitrogen-deficient g-C_3N_4. We further examined the lifetime of the charge carriers by recording time-resolved fluorescence spectra as shown in Figure 10. Both spectra decay exponentially, and the fluorescent decay kinetics of the nitrogen-deficient g-C_3N_4 are slightly slower than for g-C_3N_4. Deconvolution of the fluorescence decay spectra gives three radiative lifetimes as listed in Table 1. In both materials, the population of short-lived electron−hole pairs (less than 5 ns) is dominant (around 70%) as a result of rapid recombination of photoexcited charge carriers. Importantly, in the nitrogen-deficient g-C_3N_4, the percentage of charge carriers with a lifetime shorter than 2 ns decreases from 31.59% to 24.28%, and the percentage of charge carriers with a lifetime longer than 19 ns increases from 26.47% to 31.94%, which is certainly favorable for increasing the probability of charge carriers involved in photocatalytic reactions. The

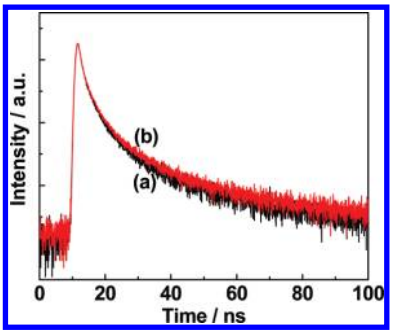

Figure 10. Time-resolved fluorescence decay spectra of the (a) g-C_3N_4 and (b) nitrogen-deficient g-C_3N_4 monitored at 470 nm by time-correlated single-photon counting. The samples were excited by incident light of 330 nm from a picosecond pulsed light emitting diode.

Table 1. Radiative Fluorescence Lifetimes and Their Relative Percentages of Photoexcited Charge Carriers in the g-C_3N_4 and Nitrogen-Deficient g-C_3N_4

sample	τ_1 (ns) − Rel %	τ_2 (ns) − Rel %	τ_3 (ns) − Rel %
g-C_3N_4	1.28 − 31.59	4.63 − 41.94	20.31 − 26.47
nitrogen-deficient g-C_3N_4	1.13 − 24.28	4.27 − 43.77	19.28 − 31.94

decreased fluorescence intensity and changed percentage of short-lived and long-lived charge carriers are apparently associated with localized states in the band gap introduced by nitrogen vacancies as revealed in Figure 6. It has been suggested that the trapping of charge carriers by the localized electronic states can retard charge carrier recombination as a consequence of reducing their spatial overlap.[32]

Many factors such as particle size, specific surface area, surface atomic structure, and electronic structure can affect the activity of photocatalysts so that it is usually difficult to exactly determine the contribution of each factor in photocatalytic activity improvement. In our case, the particle size of both materials is similar, and the nitrogen-deficient g-C_3N_4 has a little larger surface area than the g-C_3N_4 (17 vs 12 m^2 g^{-1}), which should exert a limited influence on the activity improvement shown in Figures 7 and 8. We therefore believe that the modified electronic structure plays a dominant role in improving the photocatalytic activity of nitrogen-deficient g-C_3N_4 by exerting two effects on the activity improvement: (a) suppressing the radiative recombination of charge carriers and (b) changing the population distribution of charge carriers with different lifetimes (Figure 9 and Table 1) in addition to the increased visible light absorption.

4. CONCLUSION

Nitrogen vacancies were introduced throughout the bulk of g-C_3N_4 by increasing the polycondensation temperature of the dicyandiamide precursor. The resultant nitrogen-deficient g-C_3N_4 has a slightly narrowed bandgap and extended visible light absorbance between 450 and 600 nm due to the abundant nitrogen vacancy-related C^{3+} states in the band gap. Furthermore, the radiative recombination of photoexcited charge carriers is largely restrained, and the populations of short-lived and long-lived charge carriers are decreased and increased, respectively. Consequently, the nitrogen-deficient g-C_3N_4 shows an apparently improved photocatalytic activity in

dx.doi.org/10.1021/jp301026y | J. Phys. Chem. C 2012, 116, 11013−11018

generating •OH radicals, the photodecomposition of RhB, and hydrogen evolution from water splitting.

AUTHOR INFORMATION

Corresponding Author

*E-mail: gangliu@imr.ac.cn. Fax: +86 24 23903126. Tel.: +86 24 83978238.

Notes

The authors declare no competing financial interest.

ACKNOWLEDGMENTS

The authors thank the Major Basic Research Program, Ministry of Science and Technology of China (No. 2009CB220001), NSFC (Nos. 50921004, 51002160, 21090343, 51172243), and Solar Energy Initiative of CAS for financial support. GL thanks the IMR SYNL-T.S. Kê Research Fellowship.

REFERENCES

(1) Fujishima, A.; Honda, K. *Nature* **1972**, *238*, 37−38.
(2) Chen, X. B.; Shen, S. H.; Guo, L. J.; Mao, S. S. *Chem. Rev.* **2010**, *110*, 6503−6570.
(3) Kudo, A.; Miseki, Y. *Chem. Soc. Rev.* **2009**, *38*, 253−278.
(4) Asahi, R.; Morikawa, T.; Ohwaki, T.; Aoki, K.; Taga, Y. *Science* **2001**, *293*, 269−271.
(5) Liu, G.; Wang, L. Z.; Yang, H. G.; Cheng, H. M.; Lu, G. Q. *J. Mater. Chem.* **2010**, *20*, 831−843.
(6) Kasahara, A.; Mukumizu, K.; Hitoki, G.; Takata, T.; Kondo, J. N.; Hara, M.; Kobayashi, H.; Domen, K. *J. Phys. Chem. B* **2003**, *107*, 791−797.
(7) Maeda, K.; Teramura, K.; Lu, D.; Takata, T.; Saito, N.; Inoue, Y.; Domen, K. *Nature* **2006**, *440*, 295−295.
(8) Tessier, F.; Maillard, P.; Chevire, F.; Domen, K.; Kikkawa, S. *J. Ceram. Soc. Jpn.* **2009**, *117*, 1−5.
(9) Maeda, K.; Domen, K. *J. Phys. Chem. C* **2007**, *111*, 7851−7861.
(10) Sayama, K.; Arakawa, H. *J. Photochem. Photobiol., A: Chem.* **1994**, *77*, 243−247.
(11) Hara, M.; Hitoki, G.; Takata, T.; Kondo, J. N.; Kobayashi, H.; Domen, K. *Catal. Today* **2003**, *78*, 555−560.
(12) Wang, X. C.; Maeda, K.; Thomas, A.; Takanabe, K.; Xin, G.; Carlsson, J. M.; Domen, K.; Antonietti, M. *Nat. Mater.* **2009**, *8*, 76−80.
(13) Wang, Y.; Wang, X. C.; Antonietti, M. *Angew. Chem., Int. Ed.* **2012**, *51*, 68−89.
(14) Wang, X. C.; Maeda, K.; Chen, X. F.; Takanabe, K.; Domen, K.; Hou, Y. D.; Fu, X. Z.; Antonietti, M. *J. Am. Chem. Soc.* **2009**, *131*, 1680−1861.
(15) Li, X. H.; Zhang, J. S.; Chen, X. F.; Fischer, A.; Thomas, A.; Antonietti, M.; Wang, X. C. *Chem. Mater.* **2011**, *23*, 4344−4348.
(16) (a) Yan, S. C.; Li, Z. S.; Zou, Z. G. *Langmuir* **2010**, *26*, 3894−3901. (b) Wang, Y.; Zhang, J. S.; Wang, X. C.; Antonietti, M.; Li, H. R. *Angew. Chem., Int. Ed.* **2010**, *49*, 3356−3359. (c) Liu, G.; Niu, P.; Sun, C. H.; Smith, S. C.; Chen, Z. G.; Lu, G. Q.; Cheng, H. M. *J. Am. Chem. Soc.* **2010**, *132*, 11642−11648. (d) Zhang, Y. J.; Mori, T.; Ye, J. H.; Antonietti, M. *J. Am. Chem. Soc.* **2010**, *132*, 6294−6295.
(17) (a) Yan, H. J.; Huang, Y. *Chem. Commun.* **2011**, *47*, 4168−4170. (b) Xu, X. X.; Liu, G.; Randorn., C.; Irvine, J. T. S. *Int. J. Hydrogen Energy* **2011**, *36*, 13501−13505. (c) Yan, S. C.; Lv, S. B.; Li, Z. S.; Zou, Z. G. *Dalton Trans.* **2010**, *39*, 1488−1491. (d) Wang, Y. J.; Shi, R.; Lin, J.; Zhu, Y. F. *Energy Environ. Sci.* **2011**, *4*, 2922−2929. (e) Xiang, Q. J.; Yu, J. G.; Jaroniec, M. *J. Phys. Chem. C* **2011**, *115*, 7355−7363. (f) Takanabe, K.; Kamata, K.; Wang, X. C.; Antonietti, M.; Kutoba, J.; Domen, K. *Phys. Chem. Chem. Phys.* **2010**, *12*, 13020−13025.
(18) Nowotny, M. K.; Sheppard, L. R.; Bak, T.; Nowotny, J. *J. Phys. Chem. C* **2008**, *112*, 5275−5300.
(19) Gong, X. Q.; Selloni, A.; Batzill, M.; Diebold, U. *Nat. Mater.* **2006**, *5*, 665−670.
(20) Justicia, I.; Ordejon, P.; Canto, G.; Mozos, J. L.; Fraxedas, J.; Battiston, G. A.; Gerbasi, R.; Figueras, A. *Adv. Mater.* **2002**, *14*, 1399−1402.
(21) Nakamura, I.; Negishi, N.; Kutsuna, S.; Ihara, T.; Sugihara, S.; Takeuchi, K. *J. Mol. Catal. A: Chem.* **2000**, *161*, 205−212.
(22) Liu, G.; Yang, H. G.; Wang, X. W.; Cheng, L. N.; Lu, H. F.; Wang, L. Z.; Lu, G. Q.; Cheng, H. M. *J. Phys. Chem. C* **2009**, *113*, 21784−21788.
(23) Martyanov, I. N.; Uma, S.; Rodrigues, S.; Klabunde, K. J. *Chem. Commun.* **2004**, 2476−2477.
(24) Goettmann, F.; Fischer, A.; Antonietti, M.; Thomas, A. *Angew. Chem., Int. Ed.* **2006**, *45*, 4467−4471.
(25) Lotsch., B. V.; Doblinger, M.; Sehnert, J.; Seyfarth, L.; Senker, J.; Oeckler, O.; Schnick, W. *Chem.—Eur. J.* **2007**, *13*, 4969−4980.
(26) Thomas, A.; Fischer, A.; Goettmann, F.; Antonietti, M.; Muller, J. O.; Schlogl, R.; Carlsson, J. M. *J. Mater. Chem.* **2008**, *18*, 4893−4908.
(27) Bojdys, M. J.; Muller, J. O.; Antonietti, M.; Thomas, A. *Chem.—Eur. J.* **2008**, *14*, 8177−8182.
(28) Qiu, Y.; Gao, L. *Chem. Commun.* **2003**, 2378−2379.
(29) Cronemeyer, D. C. *Phys. Rev.* **1959**, *113*, 1222−1226.
(30) Hoffmann, M. R.; Martin, S. T.; Choi, W.; Bahnemann, D. W. *Chem. Rev.* **1995**, *95*, 69−96.
(31) Hirakawa, T.; Nosaka, Y. *Langmuir* **2002**, *18*, 3247−3254.
(32) Daude, N.; Gout, C.; Jouanin, C. *Phys. Rev. B* **1977**, *15*, 3229−3235.